Direct comparison of kilohertz- and megahertz-repetition-rate femtosecond damage threshold

B. J. Nagy,[1] L. Gallais,[2] L. Vámos,[1] D. Oszetzky,[1] P. Rácz,[1] and P. Dombi[1,*]

[1]*MTA "Lendület" Ultrafast Nanooptics Group, Wigner Research Centre for Physics, 1121 Budapest, Hungary*

[2]*Aix-Marseille Université, CNRS, Centrale Marseille, Institut Fresnel, Campus de St. Jérôme, 13013 Marseille, France*

**Corresponding author: dombi.peter@wigner.mta.hu*

Received February 25, 2015; revised April 28, 2015; accepted May 4, 2015;
posted May 5, 2015 (Doc. ID 235159); published May 21, 2015

We performed femtosecond laser-induced damage threshold (fs LIDT) measurements with substantially different repetition rate Ti:sapphire laser systems: a 1 kHz regenerative amplifier and a 4.3 MHz long-cavity oscillator. All other pulse parameters are kept the same. Comparative measurements of a dielectric high reflector, a chirped mirror, and metallic mirrors show at least a factor of 2.7 lower fs LIDT at megahertz repetition rates. We attribute this to thermally assisted damage mechanisms supported by complex heat transfer simulations.

OCIS codes: (140.3330) Laser damage; (230.4040) Mirrors; (320.7090) Ultrafast lasers.
http://dx.doi.org/10.1364/OL.40.002525

In recent years, the research of femtosecond laser-induced damage threshold (fs LIDT) has grown fast as different types of femtosecond lasers have become widely available. One can distinguish single-shot and multishot LIDT measurements. Multishot studies are typically limited to repetition rates in the hertz–kilohertz (Hz–kHz) domain with different samples [1–16], providing a huge amount of useful data for femtosecond laser developers up to kilohertz (kHz) repetition rates. Data on high reflectors (HRs) versus chirped mirrors (CMs) [8], round-robin experiments with different facilities [9], and single measurements on different types of HRs and CMs [10] are all available. Systematic repetition rate dependence comparisons are also abundant in the Hz–kHz range, showing results either without any significant changes or trends in fs LIDT [17,18] or with a slightly decreasing LIDT trend toward a higher repetition rate [19]. However, due to obvious reasons, in the past development of femtosecond laser technology, kilohertz–megahertz (kHz–MHz) damage comparisons have not been targeted.

As a parallel development, MHz-repetition-rate femtosecond lasers with relatively high pulse energy have emerged recently, e.g., passively mode-locked Yb thin-disk lasers [20–22] and femtosecond fiber chirped pulse amplification systems [23]. Therefore, it is important to investigate the fs LIDT in this regime and directly compare it to standard kHz results. A measurement with a 100 MHz repetition rate oscillator on a HR mirror with a very tightly focused beam [24] and a round-robin measurement comparing this result with kHz-repetition-rate measurements have been reported, but the drawback is that several parameters of the sample illumination differ significantly [25]. Angelov *et al.* presented kHz–MHz comparison with an unknown number of pulses using a picosecond source, observing up to a factor of 2 difference depending on the material bandgap [26,27]. Therefore, it is of utmost importance to perform a direct comparison fulfilling the following requirements: (i) it studies the femtosecond damage on relevant optics (ii) between kHz- and MHz-repetition-rate illumination and (iii) has every other pulse parameter well controlled and unchanged. To the best of our knowledge, our current Letter presents such results for the first time.

To this end, we performed such measurements with kHz- and MHz-repetition-rate lasers under exactly the same conditions and performed simulations to understand the underlying mechanisms of the observed difference. We took special care to provide exactly the same conditions for damage, which includes fixing the sample, wavelength, focal spot size, pulse length, and number of interacting pulses and changing strictly only the repetition rate.

For these tests, we used two laser systems. First, we utilized a Ti:sapphire regenerative amplifier (RA) operating at 1 kHz repetition rate with 795 nm central wavelength, then we used a home-built long-cavity Ti:sapphire oscillator (LCO) at 4.3 MHz repetition rate with 805 nm central wavelength. Otherwise, the pulse parameters used for the damage tests are the same for both cases. The pulse length was 120 ± 10 fs, which was the transform-limited output of the LCO. In the case of the RA, this pulse length was achieved by chirping the 40 fs amplifier output to 120 fs with the built-in compressor grating pair. The $1/e^2$ diameter of the beam focused to the sample was 9.8 ± 0.5 μm, achieved by an 18 mm focal length aspheric lens in both cases [Fig. 1(a)]. When we consider possible displacement of the sample with respect to the focus, we arrive at a spot size deviation of ± 0.2 μm, which leads to a smaller error than the precision of the diameter measurement.

Different power levels were set by a wheel density filter. The number of pulses interacting with the sample was adjusted with a shutter with a minimum opening time of around 9 ms, which led to approximately 35,000 pulses of the LCO on the sample. Exactly the same number of pulses was applied on the sample with the shutter in the case of the RA, too. The damage event was detected visually with a stereomicroscope with 3× magnification and a CCD camera as shown in Figs. 1(b)–1(e). As the damage spot was very small and only visible on a few pixels, the method used was not able to determine *in situ* what kind of permanent alteration was caused. An independent measurement with a white-light interferometric microscope confirmed that these spots were ablations in all cases. We applied normal incidence and the sample was placed on an *xyz* translation stage.

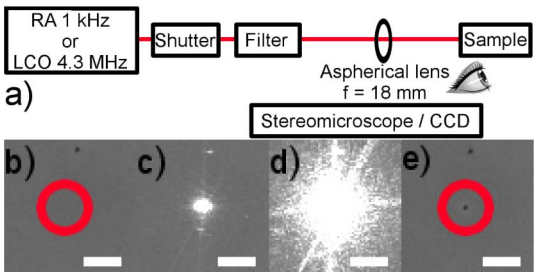

Fig. 1. (a) Scheme of the experimental setup: a regenerative Ti:sapphire amplifier (RA) and a long-cavity oscillator (LCO) with around 800 nm wavelength, a shutter with a minimum opening time of 9 ms, and a continuously variable neutral density filter wheel; the sample is on a 3D translation stage. (b) CCD image before damage, (c) during irradiation with below-threshold fluence, and (d) after only a 0.01 J/cm^2 fluence increase. Panel (e) shows the damaged spot on the HR mirror. The damage is obviously indicated by the highly increased scatter. The scale bar is 100 μm long.

We performed our measurements with both lasers as follows: we irradiated one spot with a low-power train of 35,000 pulses. We then increased the power and irradiated the same spot again until we observed the damage event, as illustrated in Figs. 1(b)–1(e). One step increase in the power corresponded to 0.01 J/cm^2 in average. The damage threshold for this particular spot is evaluated as the mean of the last power applied without damage and the first power value causing damage. This measurement is then repeated at least five times on different parts of the same sample. The final LIDT of the sample is calculated as the average of the thresholds of the individual spots. The error is given by the standard deviation of this set of LIDT values. We give the LIDT in units of peak fluence (F), which can be calculated from the average power (P), repetition rate (f), and beam area at $1/e^2$ (A) in the form $F = 2P/fA$. The prefactor of 2 emerges due to the assumption of an approximately Gaussian spatial distribution of the beam intensity in the waist.

We tested metal and dielectric mirrors, as well as CMs, representing the most relevant cases for femtosecond technology. The metal mirrors are protected gold and protected silver mirror samples both with an approximately 100 nm SiO_2 protective overcoat. The metal layer of both mirrors has a thickness of around 1 μm on a fused silica substrate. The dielectric mirror is a HR centered at 800 nm. This mirror is a $(LH)^{24}$ layer stack with the TiO_2–SiO_2 layer pair repeated 24 times. L denotes the SiO_2 ($n = 1.44$) low-index and H the TiO_2 ($n = 2.3$) high-index material. We will refer to this mirror as HR800 henceforth.

The LIDT measurement results are summarized in Table 1, with damage fluences given as F_{kHz} and F_{MHz}. Most remarkably, we can observe a F_{kHz}/F_{MHz} of between 2.7 and 4.8 in all cases representing a substantially decreasing LIDT trend for high repetition rates.

As the measurement procedure uses the same irradiated spot until the damage event, incubation effects could occur. We estimate that this leads to only a few percent deviation of the data as for high pulse numbers, increasing the pulse number further does not influence the LIDT significantly [28].

Table 1. Damage Threshold Fluence Values for kHz and MHz Repetition Rates and their Ratios

	Threshold Fluence (F) (J/cm^2)		
Sample	1 kHz	4.3 MHz	F_{kHz}/F_{MHz}
Prot. Ag mirror	0.79 ± 0.11	0.17 ± 0.01	4.8
Prot. Au mirror	0.42 ± 0.02	0.14 ± 0.01	3.0
HR800 mirror	0.28 ± 0.02	0.10 ± 0.01	2.7
Chirped mirror	0.19 ± 0.02	0.04 ± 0.01	4.8

We also have to consider the effect caused by chirping the pulse from the RA to achieve the same pulse length as that of the LCO. The bandwidth of the RA is 60 nm centered at 800 nm. As the bandgaps of the SiO_2 and TiO_2 are 6.3 and 3.5 eV, respectively, five- and three-photon ionizations can occur at SiO_2 and TiO_2, respectively. We introduced a negative chirp with the grating, which leads to an increase of the photoionization rate [29,30], decreasing the LIDT. It is known that a difference of 20% in the fs LIDT can be caused by positively and negatively chirped pulses [31]. Even though this effect could also play a role here, leading to some 20%–30% difference in the LIDT values, the observed difference by a factor of 2.7–4.8 (Table 1) definitely cannot be explained by the slight chirp introduced in the RA case. In conclusion, the measured differences remain valid.

We also note that the measured difference between the metallic and HR mirrors is different from that in a previous study [32]. Here, however, we tested protected metal mirrors, which can explain the observation.

Therefore, we concluded that thermal accumulation effects and thermally assisted femtosecond damage play a role in the observed difference in the kHz- and MHz-repetition-rate damage thresholds. As the delay between two consecutive pulses is substantially different in the kHz and MHz cases, the thermal relaxation differs significantly. To give a theoretical background for this and to confirm this assumption, we performed different simulations involving the most important underlying thermal mechanisms.

In a first approach, the thermal relaxation between two pulses was investigated. The objective was to evaluate the heat accumulation that can occur as a function of sample design (multilayer stack with and without metallic layers) and irradiation condition (kHz versus MHz repetition rates and the effect of the use of a tightly focused beam in the experiments). For simulations, we used the finite-element method with the COMSOL multiphysics software [33], considering heat transfer by conduction in solid materials. To solve the case of metal mirrors, a two-temperature model (TTM) [34] was implemented in the software, under two-dimensional (2D) axisymmetric conditions. It describes the energy transfer and the temperatures of electrons and lattice in a multilayer stack system exposed to laser irradiation at the femtosecond time scale, considering that energy is deposited in the metal film. The experimental conditions are used for the simulations (sample design and irradiation conditions). The material parameters for the metal and dielectric films that were used, and particularly their temperature dependence is described in Ref. [35]. The size of the domain was chosen to be sufficiently large, typically,

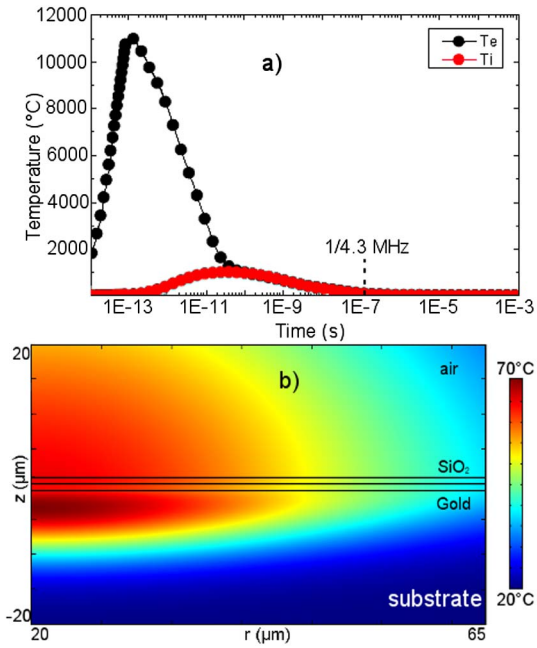

Fig. 2. Two-temperature model (TTM) finite-element simulations of a protected gold mirror (fused silica substrate–gold–SiO_2 film–air) irradiated by a 1.2 J/cm^2, 90 fs, 800 nm, 10 μm diameter laser pulse. (a) Electronic (Te) and lattice (Tl) temperature at the center of the irradiated area ($r = 0$) and at the surface of the gold film ($z = 0$). (b) Lattice temperature distribution at $t = 2.3$ μs after irradiation.

millimeter dimensions, to not have a temperature increase near the boundaries where insulation conditions were applied. An example of the simulation results for the case of the gold mirror is presented in Fig. 2.

With this model, the case of metal–dielectric stacks can be treated, provided that absorption of energy occurs in the metal. We report in Fig. 3 the thermal relaxation sequence on the metallic mirrors under study. For the case of multidielectric stacks however, the energy deposition mechanism involves complex photoionization processes that are not described in the model developed in the framework of this study. Nevertheless, qualitative simulations can be conducted in these structures. Indeed in the case of ultrashort pulse irradiation, the energy is deposited in a very short time compared with the thermal diffusion one. Therefore, we have considered thermal simulations in dielectric stacks where energy is deposited instantaneously in the material: the maximum temperature T_{max} is reached at time $t = 0$ s at the location of energy absorption (upper TiO_2 layer in the case of the HR800 mirror). By setting an initial condition of T_{max}, with a Gaussian distribution of the initial temperature (with a diameter of 10 μm, corresponding to the experiments), we calculated the evolution of the temperature in the structure for times $t > 0$ s. The results are plotted in Fig. 3.

For the metallic mirrors, in the conditions of the experiments with a focused beam, it is clear that thermal accumulation can occur for the 4.3 MHz pulse repetition rate since the material has not enough time to cool down between two pulses: the temperature increase of the gold film is 3.5°C after one pulse at 0.14 J/cm^2 and for silver these values are 1.5°C at 0.17 J/cm^2. Thermal accumulation therefore plays a main role in the damage process

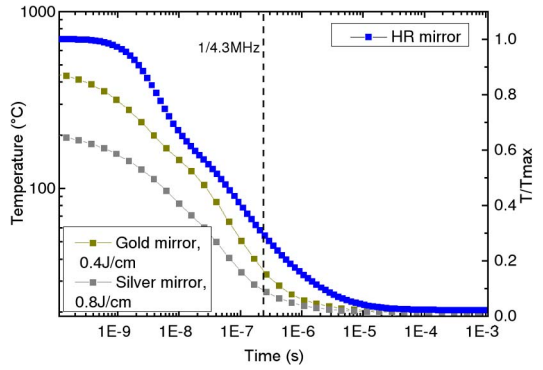

Fig. 3. Thermal relaxation after an energy deposit at time $t = 0$ s in the protected metal mirrors and in the dielectric HR mirror. In the first case, the temperature evolution (left scale) is calculated using the 2D TTM with conditions representative of the experiments (fluence, pulse length, spot size). In the HR mirror case, we considered an energy deposit in the TiO_2 layer and calculated the normalized temperature evolution (right scale).

for metal/dielectrics since an increase of a few degrees by a single pulse can lead to a dramatic increase after thousands of pulses. In the case of dielectric designs, the behavior is the same, as shown by the qualitative simulations, and thermal effects are expected to play a main role at 4.3 MHz. The situation is very different at 1 kHz because in the case of focused-beam irradiation, the material can cool down (increase of temperature is less than 0.01°C) because of radial heat transfer, and consequently, thermal accumulation is not expected to have a significant effect in the laser damage process.

To go further in this analysis, we have evaluated the theoretical LIDT in the metallic samples and its evolution under repetitive pulses. However, because of the large number of pulses that were applied, computations of 2D simulations were not possible and we changed here to a simpler 1D model, the details of which are described in Ref [35]. The 1D model does not take into account the focused beam case and radial heat transfers, and therefore, the LIDT is overestimated. The results of the simulation are given in Fig. 4 for gold and silver.

In the case of 1 kHz irradiation, and as stated before, no significant decrease of LIDT with pulse number is expected as a consequence of thermal effects. For the 4.3 MHz pulse repetition rate, a severe thermal accumulation effect is expected. After 10,000 shots, the LIDT drops to one-twentieth of the single-pulse value. This ratio has to be compared to the factor of 4.8 and 3.0 obtained for silver and gold, respectively, in the experiments (Table 1). The values calculated with the TTM model clearly overestimate the drop in LIDT because in the experimental conditions there are heat losses in the radial direction that are not taken into account in these simulations; therefore, the decrease is overestimated and should occur at a slower rate for a focused beam. However, damage mechanisms leading to substantially different observed LIDT values are well explained by the thermally assisted femtosecond damage model.

In conclusion, we have performed several LIDT measurements on typical femtosecond optics with 1 kHz and

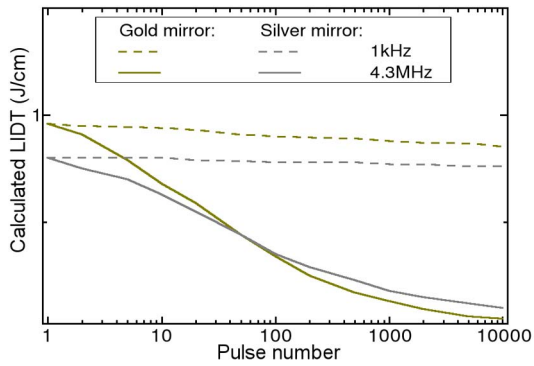

Fig. 4. Calculation of the fluence needed to reach the melting point of the metal film in the case of gold and silver mirrors irradiated at 1 kHz and 4.3 MHz repetition rates.

4.3 MHz repetition rates. We measured a substantial LIDT decrease for the MHz laser, reaching factors between 2.7 and 4.8. We identified that the huge LIDT drop at higher repetition rates is caused by thermal relaxation and heat transfer, as supported by thermal simulations of different samples. These results are crucial for the design and development of state-of-the-art high-power, high-repetition-rate femtosecond laser systems.

We thank F. Kárpát (Optilab Ltd.) for discussions and V. Pervak for the CM sample. Support was granted by the Hungarian Academy of Sciences (“Lendület”) and the National R&D&I Office, Hungary (OTKA project 109257), as well as the Max Planck Society (Partner Group Grant).

References

1. J. Krüger, D. Dufft, R. Koter, and A. Hertwig, Appl. Surf. Sci. **253**, 7815 (2007).
2. N. Sanner, O. Uteza, B. Chimier, M. Sentis, P. Lassonde, F. Legare, and J. C. Kieffer, Appl. Phys. Lett. **96**, 071111 (2010).
3. M. Mero, A. Sabbah, J. Zeller, and W. Rudolph, Appl. Phys. A **81**, 317 (2005).
4. B. Chimier, O. Utéza, N. Sanner, M. Sentis, T. Itina, P. Lassonde, F. Légaré, F. Vidal, and J. C. Kieffer, Phys. Rev. B **84**, 094104 (2011).
5. A. Couairon, L. Sudrie, M. Franco, B. Prade, and A. Mysyrowicz, Phys. Rev. B **71**, 125435 (2005).
6. O. Uteza, B. Bussière, F. Canova, J.-P. Chambaret, P. Delaporte, T. Itina, and M. Sentis, Appl. Surf. Sci. **254**, 799 (2007).
7. X. Wang, G. Lim, H. Zheng, F. Ng, W. Liu, and S. Chua, Appl. Surf. Sci. **228**, 221 (2004).
8. S. Chen, P. Gao, Y. Zhao, Y. Wang, Z. Fang, Y. Leng, and J. Shao, Appl. Opt. **53**, 3347 (2014).
9. K. Starke, D. Ristau, S. Martin, A. Hertwig, J. Krüger, P. Allenspacher, W. Riede, S. Meister, C. Theiss, A. J. Sabbah, W. G. Rudolph, V. Raab, R. Grigonis, T. Rakickas, and V. Sirutkaitis, Proc. SPIE **5273**, 388 (2004).
10. K. Starke, T. Gross, and D. Ristau, Proc. SPIE **4347**, 528 (2001).
11. D. N. Nguyen, L. A. Emmert, P. Schwoebel, D. Patel, C. S. Menoni, M. Shinn, and W. Rudolph, Opt. Express **19**, 5690 (2011).
12. D. Gómez and I. Goenaga, Appl. Surf. Sci. **253**, 2230 (2006).
13. M. Lenzner, J. Krüger, S. Sartania, Z. Cheng, C. Spielmann, G. Mourou, W. Kautek, and F. Krausz, Phys. Rev. Lett. **80**, 4076 (1998).
14. A. Wynne and B. Stuart, Appl. Phys. A **76**, 373 (2003).
15. R. Stoian, M. Boyle, A. Thoss, A. Rosenfeld, G. Korn, I. V. Hertel, and E. E. B. Campbell, Appl. Phys. Lett. **80**, 353 (2002).
16. M. Jupé, L. Jensen, A. Melninkaitis, V. Sirutkaitis, and D. Ristau, Opt. Express **17**, 12269 (2009).
17. M. Mero, D. Ristau, J. Krüger, S. Martin, K. Starke, B. Clapp, J. C. Jasapara, W. Kautek, and W. Rudolph, Opt. Eng. **44**, 051107 (2005).
18. A. Hertwig, S. Martin, J. Krüger, and W. Kautek, Thin Solid Films **453**, 527 (2004).
19. J. Bonse, S. Baudach, W. Kautek, E. Welsch, and J. Krüger, Thin Solid Films **408**, 297 (2002).
20. S. V. Marchese, C. R. E. Baer, R. Peters, C. Kränkel, A. G. Engqvist, M. Golling, D. J. H. C. Maas, K. Petermann, T. Südmeyer, G. Huber, and U. Keller, Opt. Express **15**, 16966 (2007).
21. H. Fattahi, H. Barros, M. Gorjan, T. Nubbemeyer, B. Alsaif, C. Teisset, M. Schultze, S. Prinz, M. Haefner, M. Ueffing, A. Alismail, L. Vámos, A. Schwarz, O. Pronin, J. Brons, X. Geng, G. Arisholm, M. Ciappina, V. Yakovlev, D. Kim, A. Azzeer, N. Karpowicz, D. Sutter, Z. Major, T. Metzger, and F. Krausz, Optica **1**, 45 (2014).
22. M. Delaigue, J. Pouysegur, S. Ricaud, C. Hönninger, and E. Mottay, Proc. SPIE **8611**, 86110J (2013).
23. C. Jocher, T. Eidam, S. Hädrich, J. Limpert, A. Tünnermann, A. V. V. Nampoothiri, W. Rudolph, D. Ristau, and K. Starke, Opt. Lett. **37**, 4407 (2012).
24. J. Jasapara, A. V. V. Nampoothiri, W. Rudolph, D. Ristau, and K. Starke, Phys. Rev. B **63**, 045117 (2001).
25. J. Bonse, S. Baudach, J. Krüger, W. Kautek, K. Starke, T. Gross, D. Ristau, W. G. Rudolph, J. C. Jasapara, and E. Welsch, Proc. SPIE **4347**, 24 (2001).
26. I. B. Angelov, M. Pechmann, M. K. Trubetskov, F. Krausz, and V. Pervak, Opt. Express **21**, 31453 (2013).
27. I. B. Angelov, M. K. Trubetskov, V. S. Yakovlev, O. Razskazovskaya, M. Gorjan, H. G. Barros, F. Krausz, and V. Prevak, Proc. SPIE **9237**, 92370H (2014).
28. D. Ashkenasi, M. Lorenz, R. Stoian, and A. Rosenfeld, Appl. Surf. Sci. **150**, 101 (1999).
29. I. B. Angelov, A. von Conta, S. A. Trushin, Z. Major, S. Karsch, F. Krausz, and V. Pervak, Proc. SPIE **8190**, 81900B (2011).
30. A. S. Arabanian and R. Massudi, J. Opt. Soc. Am. B **31**, 748 (2014).
31. J. R. Gulley, Opt. Eng. **51**, 121805 (2012).
32. E. Louzon, Z. Henis, S. Pecker, Y. Ehrlich, D. Fisher, M. Fraenkel, and A. Zigler, Appl. Phys. Lett. **87**, 241903 (2005).
33. www.comsol.com.
34. S. I. Anisimov, B. L. Kapeliovich, and T. L. Perelman, Sov. Phys. JETP **39**, 375 (1974).
35. B. Wang and L. Gallais, Opt. Express **21**, 14698 (2013).